

Complete abatement of the antibiotic ciprofloxacin from water using a visible-light-active nanostructured photoanode

Katherina Changanauqui^{a,b,**}, Enric Brillas^a, Pere Lluís Cabot^a, Hugo Alarcón^b, Ignasi Sirés^{a,*}

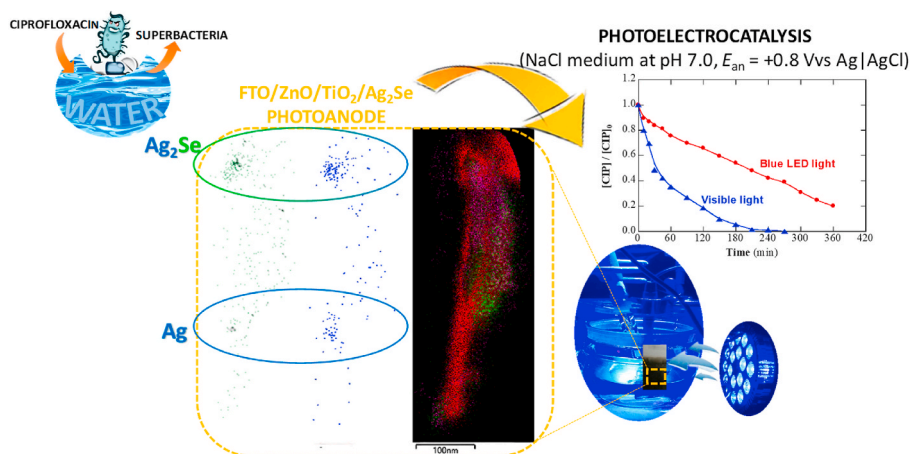
^a Laboratori d'Electroquímica dels Materials i del Medi Ambient, Departament de Ciència de Materials i Química Física, Secció de Química Física, Facultat de Química, Universitat de Barcelona, Martí i Franquès 1-11, 08028, Barcelona, Spain

^b Center for Development of Advanced Materials and Nanotechnology, Faculty of Sciences, National University of Engineering, Av. Tupac Amaru 210, Rímac, Lima, Peru

HIGHLIGHTS

- FTO/ZnO/TiO₂/Ag₂Se photoanode for water treatment by photoelectrocatalysis (PEC).
- ZnO nanorods well coated with TiO₂ and decorated with Ag₂Se and Ag nanoparticles.
- Visible-light-responsive photoanode: 100% ciprofloxacin removal in NaCl at 270 min.
- Trials with scavengers reveal a similar contribution of h_{VB}⁺ and [•]OH to oxidation.
- The photoanode is reusable: only 11% performance decay after 4 PEC trials.

GRAPHICAL ABSTRACT



ARTICLE INFO

Handling Editor: S Garcia-Segura

Keywords:

Active chlorine
Antibiotic residue
Photoelectrocatalysis
Reactive oxygen species
Visible light
Water treatment

ABSTRACT

The wide use of the fluoroquinolone antibiotic ciprofloxacin (CIP), combined with its limited removal in wastewater treatment plants, results in a dangerous accumulation in natural water. Here, the complete degradation of CIP by photoelectrocatalysis (PEC), using an FTO/ZnO/TiO₂/Ag₂Se photoanode that is responsive to blue light, has been investigated. A slow antibiotic concentration decay was found in 0.050 M Na₂SO₄ under the oxidizing action of holes and [•]OH photogenerated at the anode surface. The degradation was strongly enhanced in 0.070 M NaCl due to mediated oxidation by electrogenerated active chlorine. The latter process became faster at pH 7.0, with total abatement of CIP at concentrations below 2.5 mg L⁻¹ operating at a bias potential of +0.8 V. The performance was enhanced when increasing the anodic potential and decreasing the initial drug content. The use of solar radiation from a simulator was also beneficial, owing to the greater lamp power. In contrast, the electrochemical oxidation in the dark yielded a poor removal, thus confirming the critical role of oxidants formed

* Corresponding author.

** Corresponding author. Laboratori d'Electroquímica dels Materials i del Medi Ambient, Departament de Ciència de Materials i Química Física, Secció de Química Física, Facultat de Química, Universitat de Barcelona, Martí i Franquès 1-11, 08028, Barcelona, Spain.

E-mail addresses: kachanganauqib@uni.edu.pe (K. Changanauqui), i.sires@ub.edu (I. Sirés).

<https://doi.org/10.1016/j.chemosphere.2024.141396>

Received 3 December 2023; Received in revised form 3 February 2024; Accepted 5 February 2024

Available online 10 February 2024

0045-6535/© 2024 The Authors. Published by Elsevier Ltd. This is an open access article under the CC BY-NC-ND license (<http://creativecommons.org/licenses/by-nc-nd/4.0/>).

under light irradiation. The generation of holes and $\cdot\text{OH}$ was confirmed from tests with specific scavengers like ammonium oxalate and *tert*-butanol, respectively. The prolonged usage of the photoanode affected its performance due to poisoning of its active centers by degradation by-products, although a good PEC reproducibility was obtained upon surface cleaning.

1. Introduction

Ciprofloxacin (CIP, see physicochemical properties in Table 1) is a fluoroquinolone antibiotic widely used for treating bacterial infections in animals and humans (Nkwachukwu et al., 2023). In 2020, more than 20 million of prescriptions were filled for this drug, thus becoming the 35th most used generic drug in the world and the 5th most commonly prescribed antibacterial in USA (Shrinivas and Revanasiddappa, 2015). CIP is toxic toward aquatic organisms and its persistence in natural water is a major factor that contributes to the resistance of microorganisms, a great concern for society nowadays (Mondal et al., 2018; Orimolade et al., 2020). In effluents from CIP-producing factories, concentrations as high as 50 mg L^{-1} have been detected (Hosseini et al., 2020), whereas contents up to $2.29 \mu\text{g L}^{-1}$ have been reported for treated hospital wastewater (Botero-Coy et al., 2018). Low and moderate contents have also been reported in wastewater treatment plant (WWTP) effluents, e.g., between 2.98 and $4.23 \mu\text{g L}^{-1}$ in some plants in Peru (Nieto-Juárez et al., 2021), contributing to the expansion of bacteria such as *Escherichia coli* (Cornejo et al., 2023). Since the conventional methods applied in the WWTPs are rather inefficient to remove CIP, it is necessary to develop more powerful methods to conveniently address such contamination.

Photoelectrocatalysis (PEC), a method that combines electrochemistry and the well-known photocatalysis (PC) process, is gaining relevance among the advanced oxidation processes (AOPs) for the remediation of water and wastewater polluted with emerging organic pollutants. PEC presents several technological advantages, such as the easier photocatalyst recovery, a significant reduction of the recombination of the photogenerated electron/hole pairs as compared to PC, and a high efficiency for pollutant degradation under UVA, visible or sunlight irradiation, depending on the nature of the semiconductor photoanode (Koiki et al., 2020). Unlike PC, the photoinduced electron that appears at the photoanode upon light irradiation is transported to the cathode of the electrolytic cell through an electronic circuit, which strongly increases the lifetime of holes either to directly oxidize the organic pollutants or to react with water, eventually forming hydroxyl radical ($\cdot\text{OH}$) that mediates the oxidation of the organic molecules (Palomares-Reyna et al., 2022). In addition, a comparatively smaller

quantity of physisorbed $\cdot\text{OH}$ is formed at the photoanode surface by direct water oxidation. $\cdot\text{OH}$ is the second strongest oxidant known after fluorine, and its high standard reduction potential ($E^\circ = 2.72 \text{ V|SCE}$ at pH 0 and 25°C) ensures its non-selective attack over most organics up to mineralization, i.e., conversion into CO_2 , water and inorganic ions from heteroatoms. Other weaker oxidants like superoxide (O_2^-) and H_2O_2 can also be produced in the PEC process (Orimolade et al., 2020).

At present, the PEC research focuses on the development and application of semiconductor materials that are responsive to visible light. Among them, it is noticeable the use of Bi_2WO_6 (Li et al., 2021), $\text{Cu}_2\text{O}/\text{Ag}_3\text{PO}_4$ (Koiki et al., 2021), BiVO_4 (Wang et al., 2022), composites of TiO_2 with MoS_2 (Divyapriya et al., 2022), AgBiS_2 (Parsaei-Khomami et al., 2022) or Cu_2O (Koiki et al., 2020), and ZnO-based composites with Ni (Gholami et al., 2020). Some sulfides have been applied to the PEC treatment of CIP, such as MoS_2 vertically aligned in Ti sheets, which presents improved optoelectronic properties and superior chemical stability and photostability as compared to metal oxides (Zhou et al., 2019).

ZnO and TiO_2 are the most ubiquitous and efficient photoanodes for PEC, since they show high stability, non-toxicity and low cost. Although each of them is effective under UVA light because their bandgap energy (E_{bg}) is close to 3.2 – 3.3 eV , efforts have been made to prepare ZnO/ TiO_2 composites to operate under near-visible light (Pirhashemi et al., 2018). Recently, our groups synthesized a novel ZnO/ $\text{TiO}_2/\text{Ag}_2\text{Se}$ photoanode with a low $E_{\text{bg}} = 1.85 \text{ eV}$ and good stability, resulting in a good performance regarding the removal of pharmaceuticals like oxytetracycline (Changanaqui et al., 2020b) and naproxen (Changanaqui et al., 2020a) by PEC with a blue LED lamp. The β - Ag_2Se phase behaves as an *n*-type semiconductor, being widely used as photosensitizer of thermal chromic materials because of its narrow bandgap (Helan et al., 2015). However, more research is necessary to know if this novel ZnO/ $\text{TiO}_2/\text{Ag}_2\text{Se}$ composite can be useful for the broader destruction of pharmaceuticals by PEC.

In this work, the performance of a PEC system with a ZnO/ $\text{TiO}_2/\text{Ag}_2\text{Se}$ photoanode illuminated with visible light for CIP degradation is investigated. The composite was prepared as a thin film deposited onto a transparent fluorine-based tin oxide (FTO) glass. The effect of the electrolyte composition, anodic potential (E_{an}) and CIP concentration on the degradation process was explored. The system was operated in the dark by electrochemical oxidation (EO), as well as under visible light irradiation with different lamps. The nature of the photogenerated oxidizing agents was ascertained with selected scavengers, and the reusability of the photoanode was tested in successive degradation cycles.

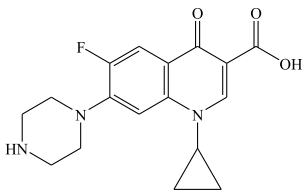
2. Materials and methods

2.1. Chemicals

Ciprofloxacin hydrochloride ($\geq 98\%$ purity) was purchased from Merck Supelco. FTO glass TEC7 wafers (2.2 mm thick, $7 \Omega \text{ sq}^{-1}$ resistance) were purchased from Dyesol Australia. Na_2SO_4 and NaCl used as supporting electrolytes were of analytical grade purchased from Fluka. The solution pH was regulated with analytical grade H_2SO_4 or HCl supplied by Merck. High-purity water (Millipore Milli-Q, resistivity $>18.2 \text{ M}\Omega \text{ cm}$) was used to prepare the solutions. Other chemicals of HPLC or analytical grade were purchased from Merck, Sigma-Aldrich and Panreac.

Table 1

Main physicochemical characteristics of ciprofloxacin.

Chemical name	1-Cyclopropyl-6-fluoro-4-oxo-7-piperazin-1-ylquinoline-3-carboxylic acid
Chemical formula	$\text{C}_{17}\text{H}_{18}\text{FN}_3\text{O}_3$
Chemical structure	
Solubility in water	36 mg mL^{-1} (25°C)
Melting point	255 – 257°C
$\log K_{\text{OW}}$	0.28 (non-ionized)
$\text{p}K_{\text{a}}$	6.09 and 8.62

2.2. Preparation of the FTO/ZnO/TiO₂/Ag₂Se electrode

The FTO/ZnO/TiO₂/Ag₂Se (photo)anode was prepared following the procedure described elsewhere (Changanaqui et al., 2020a, 2020b). In summary, the FTO substrate with a geometric area of 5 cm² was placed as the cathode of an electrolytic cell to deposit Zn(OH)₂ seeds from a 0.10 mM Zn(CH₃COO)₂ solution at 70 °C by applying a cathodic potential ($E_{\text{cath}} = -1.1 \text{ V/Ag|AgCl}$) for 180 s. After calcination at 400 °C for 2 h, the ZnO NRs were grown from the seeds in a solution at 90 °C for 75 min (Rodríguez et al., 2010). The resulting thin film made of ZnO NRs was immersed in an alkaline colloidal TiO₂ suspension to proceed with a dip-coating process. The sample was dried at 100 °C for 10 min and calcined at 550 °C for 1 h. The sequence was repeated until 3 layers were obtained. Finally, Ag₂Se NPs were electrodeposited onto the FTO/ZnO/TiO₂ composite via immersion in AgNO₃ + H₂SeO₃ solution (0.50 M KSCN, 5.0 mM AgNO₃, 2.5 mM H₂SeO₃ and 0.05 M KNO₃) at pH 3.0 and 25 °C, by applying an $E_{\text{cath}} = -0.65 \text{ V/Ag|AgCl}$ for 600 s.

2.3. Electrolytic system

The PEC assays were carried out in a conventional three-electrode undivided cell containing solutions of 100 mL, kept under vigorous magnetic stirring at 25 °C. The FTO/ZnO/TiO₂/Ag₂Se electrode prepared as explained in section 2.2 was applied as the anode or photoanode, being rinsed with Milli-Q water after each use. The cathode was a Pt wire and Ag|AgCl (KCl sat.) served as reference electrode. All the potentials given in this work are referred to this latter electrode. An Amel 2051 potentiostat-galvanostat was utilized to supply a constant E_{an} to the (photo)anode. The photoanode was illuminated with a blue LED lamp (2 × 18 W) of $\lambda = 460 \text{ nm}$ from Higrow, placed outside the cell in parallel to the photoanode surface (7 cm). The effect of the supporting electrolyte (0.070 M Na₂SO₄ or 0.070 M NaCl), pH (5.6 or 7.0), applied E_{an} (from +0.7 to +1.0 V) and CIP content (from 1.0 to 5.0 mg L⁻¹) on the performance of the PEC process was studied. Ammonium oxalate (scavenger of h_ν⁺) and *tert*-butanol (TBA, scavenger of ·OH) were added in specific trials to identify the oxidizing agents generated. Comparative experiments under EO conditions (i.e., without light irradiation) were made to characterize the FTO/ZnO/TiO₂/Ag₂Se electrode as anode. The PEC performance was also examined under solar light by exposing the anode to an LS300 Xe solar simulator from LOT-Quantum Design equipped with a high-pressure Xe arc lamp of 300 W and IR and UV cut-off filters.

2.4. Instruments and analytical methods

The atomic structure of the as-prepared ZnO/TiO₂/Ag₂Se material was ascertained by high-resolution transmission electron microscopy (HRTEM, JEOL JEM-2100) with a LaB₆ filament at 200 kV. This apparatus was equipped with an Oxford Instruments Xplore energy-dispersive X-ray spectroscopy (EDX) detector. The HRTEM images were acquired using a Gatan Orius CCD camera and the STEM HAADF images with a JEOL HAADF detector. The data were analyzed with Digital Micrograph software for HRTEM and an Aztec software for EDX mapping. Thin films of ZnO/TiO₂/Ag₂Se were analyzed by X-ray diffraction (XRD) using a PANalytical X'Pert PRO MPD Alpha1 powder diffractometer in Bragg-Brentano $\theta/2\theta$ geometry of 240 mm of radius, with Cu K α ($\lambda = 1.5406 \text{ \AA}$) radiation and 2θ scan from 20° to 70°. The oxidation states of chemical elements were characterized by X-ray photoelectron spectroscopy (XPS) with a Physical Electronic PHI 5500 Multitechnique system, with X-ray source (Al K α line of 1486.6 eV energy and 350 W) placed perpendicular to the analyzer axis.

The solution pH and conductivity were measured with a Crison 2200 pH-meter and a Metrohm 644 conductometer, respectively. The change of CIP concentration during the treatments was monitored by reverse-phase high-performance liquid chromatography (HPLC) using a Waters 600 LC coupled to a Water 996 diode array detector selected at a $\lambda =$

356 nm. The column was a Biphenyl 100 Å LC Kinetex (5 μm , 150 mm × 4.6 mm), and the mobile phase was a 40:60 (v/v) acetonitrile/0.1% formic acid mixture eluted at 0.5 mL min⁻¹. CIP was detected at a retention time of 3.9 min with a limit of detection (LOD) of 0.1 mg L⁻¹. All the trials were made in triplicate, and the average values are reported showing the error bars within a 95% confidence interval in the figures. From these results, the percentage of CIP degradation was calculated according to Eq. (1), and the corresponding pseudo-first-order kinetic analysis was done from Eq. (2):

$$\% \text{ CIP degradation} = \frac{[\text{CIP}]_0 - [\text{CIP}]}{[\text{CIP}]_0} \times 100 \quad (1)$$

$$\ln \left(\frac{[\text{CIP}]_0}{[\text{CIP}]} \right) = k_1 t \quad (2)$$

where [CIP]₀ and [CIP] denote the initial CIP concentration and that at time t (in min), respectively, and k_1 is the pseudo-first-order rate constant for CIP degradation.

Active chlorine was determined in triplicate using the *N,N*-diethyl-*p*-phenylenediamine colorimetric method with a Shimadzu 1800 UV/Vis spectrophotometer at $\lambda = 515 \text{ nm}$ (APWA, 2005).

3. Results and discussion

3.1. Characterization of the ZnO/TiO₂/Ag₂Se thin film

After two uses of the FTO/ZnO/TiO₂/Ag₂Se thin film as photoanode under PEC conditions, the material surface was scratched to be analyzed by EDX. Fig. 1a shows the presence of Zn, Ti, O, Ag, Na, and Se in the EDX spectrum. Fig. 1b depicts the distribution of these elements on the surface of a nanorod at a magnification of 200,000× for a selected scanning area. Zn, Ti and O were the most abundant elements along the nanorod wall, confirming the effective coating of TiO₂ onto the surface of the underlying ZnO nanorod. This proves the stability of the ZnO/TiO₂ thin film during the PEC treatments. In contrast, the Ag signals are not distributed along the nanorod but they accumulate in distinct near-spherical features (see upper and mid bright spots). The identification of Se signals was more difficult, but they could be found in some of those rounded spots, always associated to Ag, thus confirming the electrodeposition of nanoparticles made of Ag and Se decorating the nanorod surface. The same elements were detected in the pristine photoanode, as previously reported (Changanaqui et al., 2020b), although the presence of Na in the used material was evidenced (see Fig. 1b), which can be explained by the adsorption of Na⁺ present in the supporting electrolyte during the PEC treatment.

The diffractogram of Fig. 1c reveals the crystallinity of the ZnO/TiO₂/Ag₂Se thin-film structure, in addition to the suggested identification of each signal according to the XRD patterns of standards. The tetragonal structure of the SnO₂ substrate (JCPDS No. 41e1445) can be observed, with signals located at 26.5°, 33.6°, 37.7°, 51.4°, 54.5°, 61.6° and 65.6°. The wurtzite hexagonal structure of ZnO nanorods (JCPDS, No. 036e1451) is corroborated by the presence of signals at 31.8°, 34.3°, 36.2°, 47.4°, 56.6°, 62.8° and 67.8°, which correspond to the (100), (002), (101), (102), (110), (103) and (112) planes, respectively (Someswarao et al., 2021). The predominant signal of the (002) plane is in excellent agreement with the preferential vertical growing of the nanorods. The anatase TiO₂ structure (JCPDS No. 21e1272) is confirmed by expected signals at 25.3°, 47.8°, 53.8°, 54.9° and 68.7°, assigned to the (101), (200), (105), (211) and (116) planes (Li et al., 2014). Finally, the orthorhombic phase of Ag₂Se (JCPDS No. 04e0783) was verified from peaks at 33.6° and 35.2°, characteristic of the crystalline planes (112) and (121) (Zheng et al., 2022), which matches with the EDX results discussed above. The same crystalline compounds have been found in the pristine photoanode (Changanaqui et al., 2020b).

The general XPS spectrum of the FTO/ZnO/TiO₂/Ag₂Se thin film is

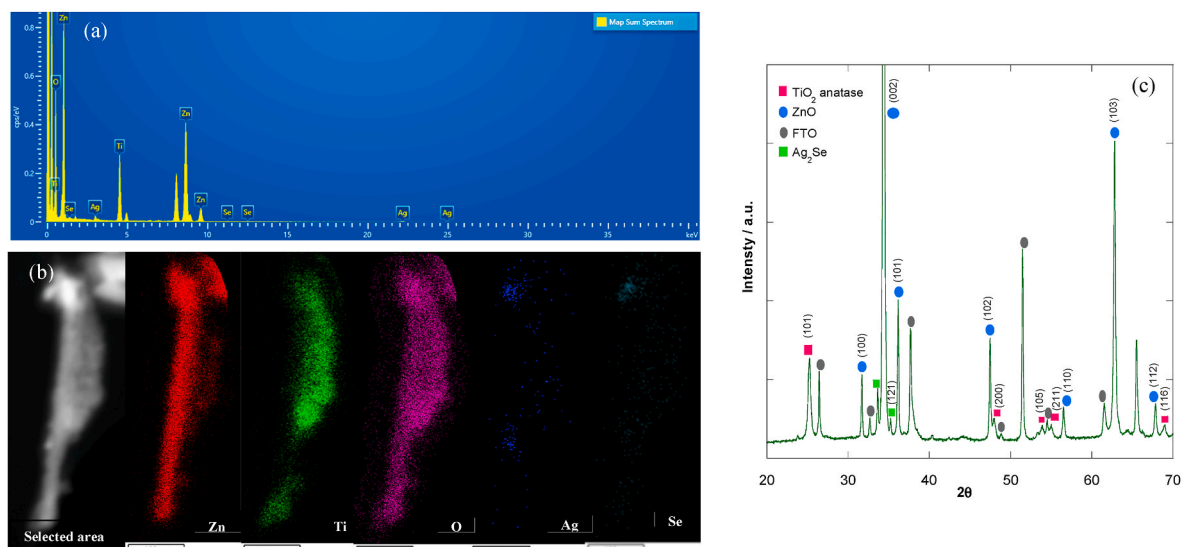


Fig. 1. (a) EDX spectrum of the as-synthesized FTO/ZnO/TiO₂/Ag₂Se photoanode thin film. (b) Elemental mapping at 200,000x, showing the selected scanning area and the distribution of Zn, Ti, O, Ag, Na, and Se in the photoanode. (c) XRD pattern of the photoanode coating.

shown in Fig. 2a, whereas those corresponding to each chemical element are depicted in Fig. 2b–f. Fig. 2b depicts the characteristic signal of Zn 2p_{3/2} at 1022.8 eV and that of the Zn 2p_{1/2} at 1045.8 eV, which agree with previous findings for ZnO nanorods (Fan et al., 2015). The signal of Ti 2p highlighted in Fig. 2c corresponds to the oxidation state of Ti(IV), with 1 energies of 459.7 and 465.4 eV related to orbitals Ti 2p_{3/2} and Ti 2p_{1/2}, very close to the values of 459.6 and 465.4 eV previously reported, respectively (Govindaraj et al., 2018). The deconvolution of the O 1s signal presented in Fig. 2d yields 4 signals at energies of: (i) 530.4

eV, related to the O²⁻ of the Ti–O bond in TiO₂ (Govindaraj et al., 2018); (ii) 531.0 eV, which can be associated with the Ag–O bond that informs about the presence of oxidized silver (Wang et al., 2020); (iii) 531.6 eV, ascribed to the O vacancies; and (iv) 532.5 eV, resulting from the surface OH of the oxide (Komtchou et al., 2018). Fig. 2e shows the deconvolution of the Ag signal, corroborating the presence of Ag₂Se (368.3 and 374.3 eV), metallic Ag (368.8 and 374.7 eV) and Ag⁺ cation (369.8 and 375.5 eV) (Changanaqui et al., 2020b). The higher relative intensity of the Ag₂Se band suggests its prevalence over Ag⁺ cation in the

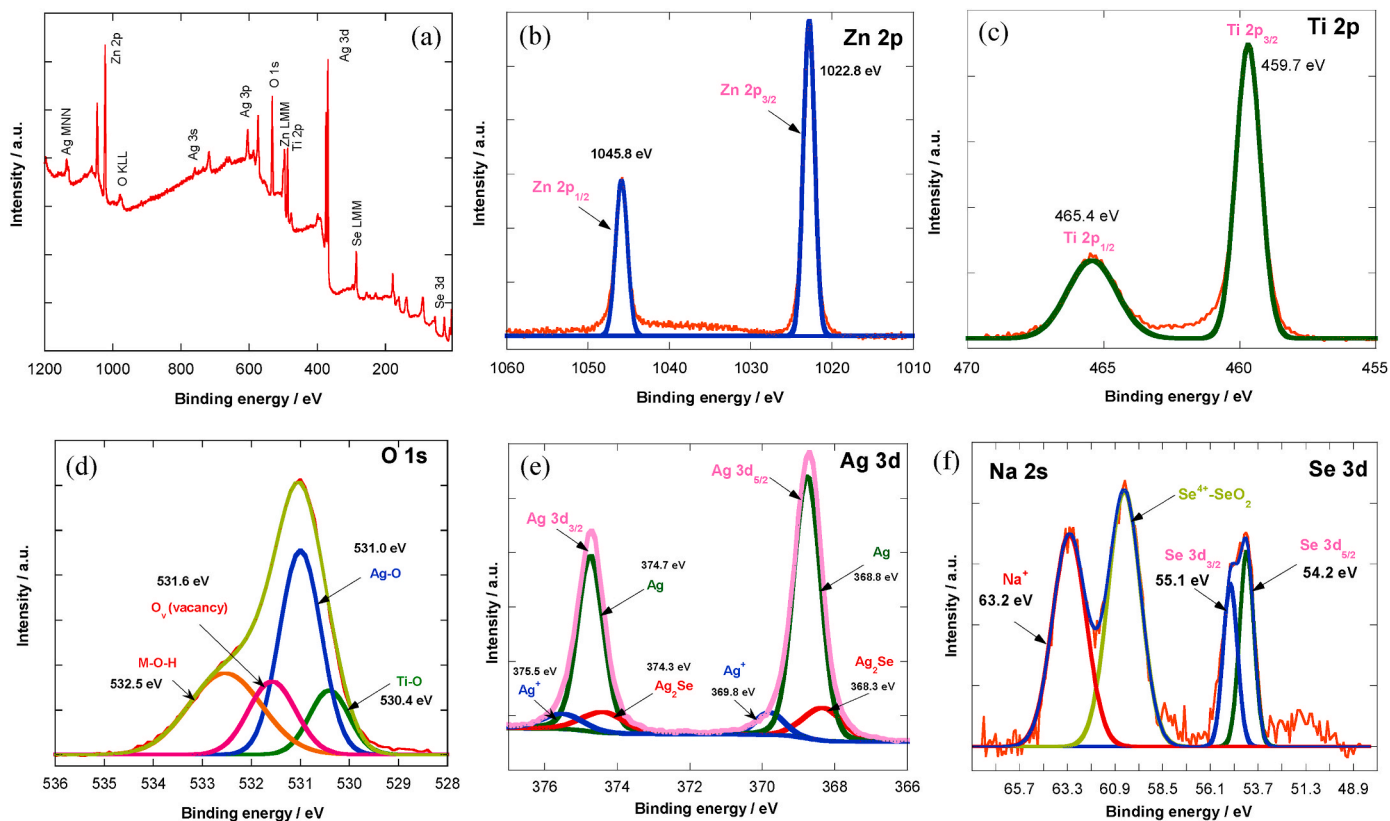
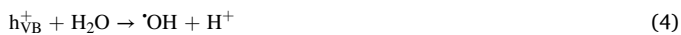


Fig. 2. (a) General XPS spectrum of the photoanode. High resolution spectra of the different elements present in the photoanode: (b) Zn 2p, (c) Ti 2p, (d) O 1s (deconvoluted), (e) Ag 3d (deconvoluted), and (f) Se 3d (deconvoluted).

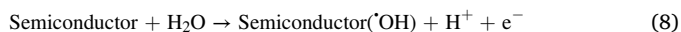
nanoparticles that decorate the surface of the ZnO/TiO₂ film. Note that the band at 356.6 eV typically associated to Ag₂O was not found (Ge et al., 2006). Finally, the signal at 54.2 eV in Fig. 2f can be related to Se 3d_{5/2}, in agreement with the presence of selenide in the form of Ag₂Se, and that of 60.0 eV corresponds to SeO₂. There is not any evidence of a signal at 55.9 eV related to pure Se (Chen et al., 2002). All these findings allow concluding that the Ag₂Se and Ag nanoparticles in the photoanode used in two runs decorated the ZnO/TiO₂ surface, although accompanied by some Ag and Se oxide, as also found for the pristine material in our previous work.

3.2. Effect of operation parameters on ciprofloxacin degradation by PEC process

In PC, a semiconductor suspended into the polluted solution is illuminated to promote the jump of an electron of its valence band (VB) to its conduction band (CB, e_{CB}⁻). This originates a hole h_{VB}⁺ in the VB by reaction (3) (Oriol et al., 2019; Brillas and Garcia-Segura, 2023). The incident photons need to provide an energy higher or equal to the E_{bg} of the semiconductor photocatalyst for the creating separated charges in the form of e_{CB}⁻/h_{VB}⁺ pairs. The latter species can then directly oxidize the organic pollutants or react with water or OH⁻ to form the oxidant [•]OH by reactions (4) or (5), respectively. In turn, the photogenerated e_{CB}⁻ can reduce dissolved O₂ to O₂⁻ from reaction (6). However, the rapid recombination of h_{VB}⁺ and e_{CB}⁻ by reaction (7) is known to cause a loss of efficiency. The main aim of PEC is solving this drawback.



PEC process is carried out in an electrolytic cell with a photoanode and a cathode, both exposed to the contaminated solution. The photoanode mainly supports the photocatalyst that is exposed to light radiation to promote the formation of the e_{CB}⁻/h_{VB}⁺ pair from reaction (3). Under the supply of an electric current, the photoexcited e_{CB}⁻ is transferred to the cathode to reduce H₂O or H⁺ to H₂ gas. This dramatically reduces the rate of the recombination reaction (7), thereby strongly prolonging the time span of the photogenerated h_{VB}⁺ and, consequently, enhancing its effective oxidation power. It is then expected that the degradation of organic pollutants proceeds through the action of this species and [•]OH generated from reactions (4) or (5). Moreover, physisorbed [•]OH, denoted as semiconductor([•]OH), is originated by water discharge from reaction (8) (Brillas and Garcia-Segura, 2023), potentially contributing to the destruction of organic molecules.



Other strong oxidants can be formed depending on the electrolyte composition. To investigate this behavior with the as-prepared FTO/ZnO/TiO₂/Ag₂Se photoanode illuminated with a 36-W blue LED lamp, 100 mL of solutions with 5.0 mg L⁻¹ CIP and 0.050 M Na₂SO₄ or 0.070 M NaCl at natural pH 5.6 and 25 °C were treated by PEC at E_{an} = +0.8 V. Note that both media had the same conductivity of 7.50 mS cm⁻¹, to make the trials comparable in terms of ion migration. Fig. 3a depicts a slow and gradual decay of the antibiotic concentration in both cases, attaining 60% and 69% degradation after 390 min of electrolysis in the sulfate and chloride medium, respectively. The quicker abatement obtained in 0.070 M NaCl can be explained by the generation of another strong oxidant such as active chlorine (Cl₂/HClO/ClO⁻) from reactions (9)–(11) (dos Santos et al., 2020; Murrieta et al., 2020). The Cl⁻ anion of the electrolyte is oxidized at the photoanode by reaction (9), giving rise to Cl₂ that is subsequently hydrolyzed to HClO at pH > 3.0 by reaction

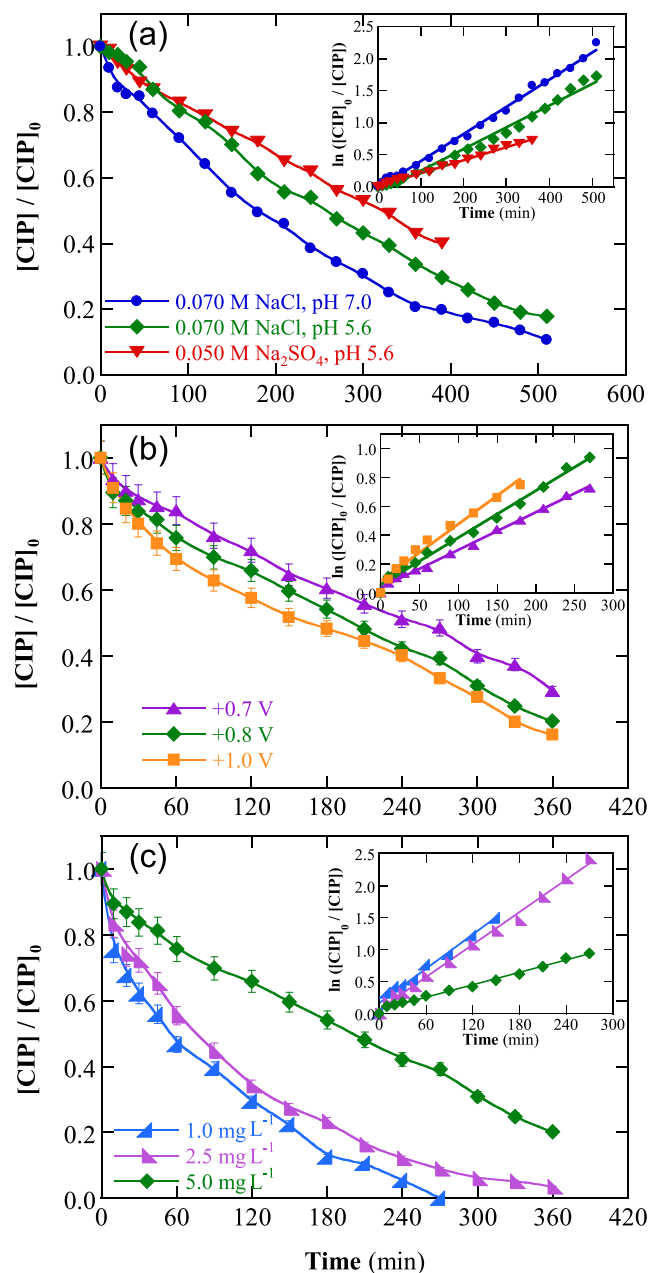
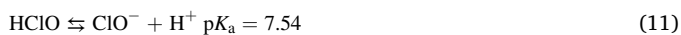


Fig. 3. Change of the normalized ciprofloxacin (CIP) concentration with electrolysis time for the photoelectrocatalytic (PEC) treatment of 100 mL of antibiotic solutions under different conditions at 25 °C using a three-electrode undivided cell with: a) FTO/ZnO/TiO₂/Ag₂Se photoanode, irradiated with a 36-W blue LED lamp ($\lambda = 460$ nm), a Pt cathode and Ag|AgCl reference electrode. Effect of: (a) electrolyte composition and pH, at 5.0 mg L⁻¹ CIP and anodic potential (E_{an}) = +0.8 V, (b) anodic potential, using 5.0 mg L⁻¹ CIP in 0.070 M NaCl at pH 7.0, and (c) antibiotic concentration in 0.070 M NaCl at pH 7.0, at E_{an} = +0.8 V. The inset panels show the corresponding pseudo-first-order kinetic analysis for CIP content decay. (For interpretation of the references to color in this figure legend, the reader is referred to the Web version of this article.)

(10). This species can then be deprotonated to ClO⁻ at pH > 8.0 via reaction (11). During all these treatments, the solution pH became more acid, dropping to a final pH near 3, in agreement with the formation of acidic by-products. It can then be established that HClO is the main chlorine agent acting under the current electrolytic conditions at pH 5.6, which is beneficial because this is the most powerful among the active

chlorine species.



The excellent pseudo-first-order kinetic analysis for the above CIP concentration abatements, performed from Eq. (1), is presented in the inset panel of Fig. 3a. Table 2 summarizes the rate constant values. A value of $k_1 = 2.14 \times 10^{-3} \text{ min}^{-1}$ was determined in Na_2SO_4 , which rose to $k_1 = 2.64 \times 10^{-3} \text{ min}^{-1}$ for trials made in NaCl.

The most powerful oxidation treatment, i.e., NaCl as the electrolyte, was subsequently tested at pH 7.0 because this is the typical value for natural water and many industrial effluents. Surprisingly, Fig. 3a discloses a more rapid CIP abatement at this more alkaline pH, reaching 80% and 90% degradation after 390 and 450 min of treatment, with a $k_1 = 3.24 \times 10^{-3} \text{ min}^{-1}$ (see Table 2). Since a similar production of oxidizing agents (h_{VB}^+ , $\cdot\text{OH}$ and HClO) is expected to be generated at both pH values, the superior performance at pH 7.0 can be associated to the presence of a more electroactive CIP species. The first $\text{p}K_a$ of CIP is 6.09 (see Table 1), being related to the deprotonation of its carboxylic acid and hence, it can be suggested that the carboxylate anion form of CIP present at pH 7.0 becomes either more easily oxidized or more easily adsorbed on the photoanode surface (positive pole in the electrolytic cell).

The effect of the applied E_{an} on the removal of 5 mg L^{-1} CIP in 0.070 M NaCl at pH 7.0 was further explored. The data given in Fig. 3b reveal an enhancement of the antibiotic decay when rising E_{an} from $+0.7$ to $+1.0 \text{ V}$, with increasing k_1 -values from 2.61×10^{-3} to $3.92 \times 10^{-3} \text{ min}^{-1}$ (see the inset panel of this figure and Table 2). This enhancement can be justified by the progressive acceleration of the formation of the oxidizing agents. At a gradually higher E_{an} , the faster extraction of e_{CB}^- originates larger amounts of reactive h_{VB}^+ and $\cdot\text{OH}$ from reactions (3) to (5), whereas the increase in rate of Cl^- oxidation by reaction (9) favors the production of HClO from reaction (10).

Fig. 3c highlights the influence of the antibiotic concentration from 1.0 to 5.0 mg L^{-1} in 0.070 M NaCl medium at pH 7.0 and $E_{\text{an}} = +0.8 \text{ V}$. A faster degradation can be observed as the CIP content decreases. At 2.5 mg L^{-1} CIP, the overall abatement was achieved at 360 min, which became quicker (240 min) when employing a lower CIP content of 1.0 mg L^{-1} . The inset panel of this figure reveals the decay of the k_1 -value from 8.95×10^{-3} to $3.24 \times 10^{-3} \text{ min}^{-1}$ with an increasing CIP concentration from 1.0 to 5.0 mg L^{-1} . This tendency can be simply related to the faster destruction at lower organic load by a similar amount of produced oxidants. However, a deeper study of the above results allows concluding that at 270 min, time at which 1.0 mg L^{-1} of the antibiotic

Table 2

Pseudo-first-order rate constants and coefficient of determination (R -squared) found for degradation trials with 100 mL of ciprofloxacin solutions in different aqueous matrices, using a three-electrode undivided cell with an FTO/ZnO/TiO₂/Ag₂Se photoanode irradiated with a 36-W blue LED lamp, a Pt cathode and Ag|AgCl reference electrode.

Method	Medium	[CIP] (mg L ⁻¹)	pH	E_{an} (V)	k_1 (10 ⁻³ min ⁻¹)	R^2
EO	0.070 M NaCl	5.0	7.0	+0.8	2.76	0.983
PEC	0.070 M Na ₂ SO ₄	5.0	5.6	+0.8	2.14	0.991
PEC	0.070 M NaCl	5.0	5.6	+0.8	2.61	0.995
PEC	0.070 M NaCl	1.0	7.0	+0.8	8.95	0.985
PEC	0.070 M NaCl	2.5	7.0	+0.8	8.45	0.995
PEC	0.070 M NaCl	5.0	7.0	+0.7	2.61	0.992
PEC	0.070 M NaCl	5.0	7.0	+0.8	3.24	0.995
PEC	0.070 M NaCl	5.0	7.0	+1.0	3.92	0.982
PEC ^a	0.070 M NaCl	5.0	7.0	+0.8	15.0	0.984

^a Using a solar simulator.

was completely removed, a much greater content of about 3.0 mg L^{-1} could be abated when treating a CIP solution at 5.0 mg L^{-1} (60% degradation). This informs about a greater oxidation power of the PEC process as the pollutant content increases, owing to the favored attack of larger quantities of oxidizing agents. A higher organic load is thus beneficial because the molecule react with oxidants, which limits their waste in parasitic reactions. Examples of such unwanted reactions for $\cdot\text{OH}$ are its dimerization to H_2O_2 by reaction (12) and its consumption by HClO via reaction (13). In turn, HClO can be transformed by Cl^- from reaction (14) (Murrieta et al., 2020):



3.3. Comparison of ciprofloxacin degradation in different systems

The PEC treatment of CIP with an FTO/ZnO/TiO₂/Ag₂Se photoanode was compared with an analogous EO process (i.e., without light irradiation) to know the oxidation power of the semiconductor ($\cdot\text{OH}$) species formed from reaction (8) and HClO produced from reactions (9) and (10). This assay was made with 5.0 mg L^{-1} CIP in 0.070 M NaCl medium at pH 7.0, 25°C and $E_{\text{an}} = +0.8 \text{ V}$, and the decay of the normalized antibiotic concentration is shown in Fig. 4a. A very slow degradation can be observed, with 32% of destruction at 360 min, which is much smaller than the 80% concentration abatement found in the PEC treatment with the 36-W blue LED lamp. However, the k_1 -value for the EO process was as high as $2.76 \times 10^{-3} \text{ min}^{-1}$, although certainly only for the first 60 min of treatment (see Fig. 4b and Table 2), whereupon the linearity of the pseudo-first-order kinetics disappeared. This fact points to consider that h_{VB}^+ formed from reaction (3) and $\cdot\text{OH}$ mainly formed from reaction (4) are the main oxidizing agents in the PEC process. The antibiotic decay by EO in chloride medium can then be ascribed to the main oxidative action of HClO, which influences the PEC process as stated above.

The viability of the FTO/ZnO/TiO₂/Ag₂Se photoanode in PEC treatments with solar irradiation was explored to show its potential application with a free energy source. To do this, the photoanode was exposed to a high-pressure Xe arc lamp of 300 W that provided radiation with λ between 250 and 2500 nm, although the effective emission was limited to the visible light range using filters. Fig. 4a depicts the fast degradation undergone by 5.0 mg L^{-1} CIP solution in 0.070 M NaCl at pH 7.0, 25°C and $E_{\text{an}} = +0.8 \text{ V}$ in this system. Under these conditions, total CIP abatement was reached in 270 min with a $k_1 = 1.5 \times 10^{-2} \text{ min}^{-1}$ (see Fig. 4b and Table 2), i.e., a much better performance than that determined with the blue LED lamp. This can be accounted for by the higher energy of the Xe lamp, along with the absorbance of a wider range of visible photons beyond blue. As a result, the photogeneration of $\text{e}_{\text{CB}}^-/\text{h}_{\text{VB}}^+$ pairs from reaction (3) is accelerated. For this assay, a gradual accumulation of active chlorine concentration up to 0.58 mg L^{-1} (i.e., 0.011 mM) at 240 min was determined, as shown in Fig. 4c, suggesting a slow attack of this oxidant over CIP and its by-products. However, no TOC reduction was found under these conditions, which can be related to the formation of recalcitrant chloroderivatives upon the attack of active chlorine.

3.4. Effect of scavengers and detection of main generated oxidants

A series of assays with specific scavengers was carried out to detect the oxidizing agents in the PEC treatment with an FTO/ZnO/TiO₂/Ag₂Se photoanode irradiated with blue LED light. Concentrations of 7 mM of ammonium oxalate or 500 mM of TBA were added to the 5.0 mg L^{-1} CIP $+0.070 \text{ M NaCl}$ solution at pH 7.0 and 25°C , and $E_{\text{an}} = +0.8 \text{ V}$ was applied during 360 min. Ammonium oxalate acts as a specific scavenger

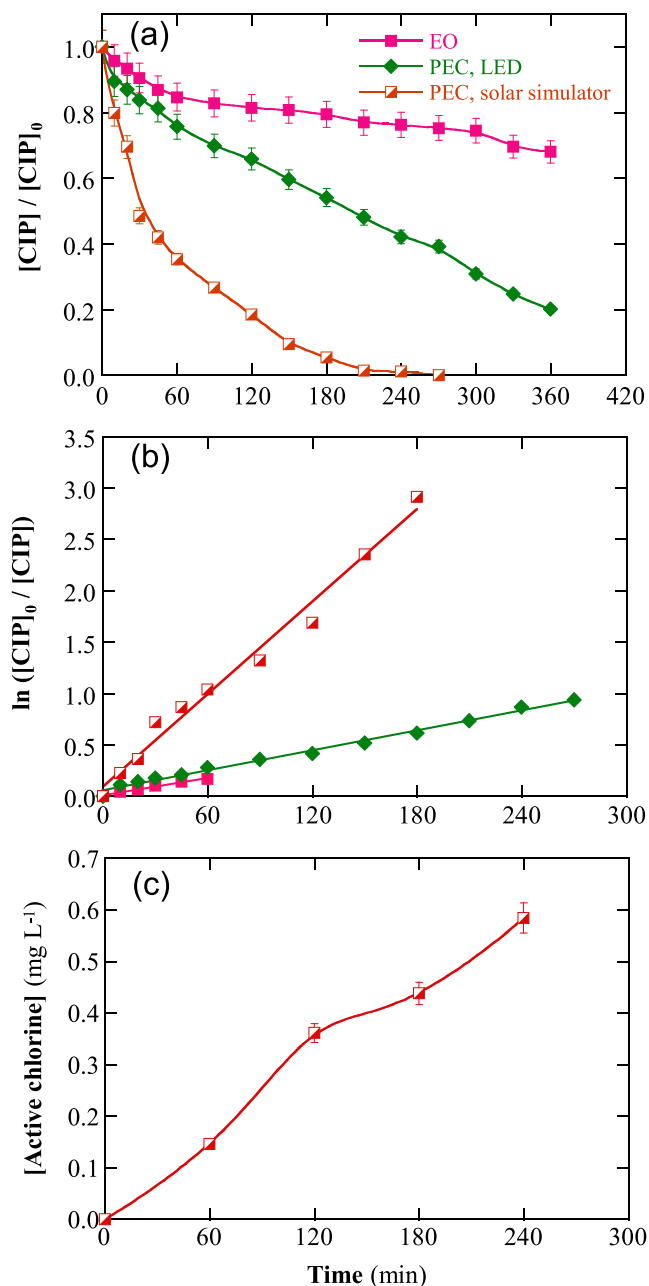


Fig. 4. (a) Variation of the normalized CIP concentration with electrolysis time for the treatment of 100 mL of 5.0 mg L^{-1} CIP in 0.070 M NaCl medium at pH 7.0, 25°C and $E_{\text{an}} = +0.8 \text{ V/Ag|AgCl}$ by: electrochemical oxidation (EO), PEC with irradiation from a 36-W blue LED lamp and PEC with a solar simulator. The system was as that of Fig. 3, with a FTO/ZnO/TiO₂/Ag₂Se anode/photoanode. (b) Pseudo-first-order kinetic analysis of the above concentration abatements. (c) Evolution of generated active chlorine during PEC with a solar simulator. (For interpretation of the references to color in this figure legend, the reader is referred to the Web version of this article.)

of the h_{VB}^+ species, and its concentration was taken from Zhang et al. (2011) and Lin et al. (2012), whereas TBA only consumes the $\cdot\text{OH}$ radicals, being its concentration previously explored by dos Santos et al. (2021). Fig. 5a depicts that at the end of these trials, CIP concentration decay was only 54–55%, a value more than 30% poorer than that attained without scavengers (79.9%). This confirms the generation of a similar proportion of reactive h_{VB}^+ and $\cdot\text{OH}$ from reactions (3) and (4), respectively. No deeper CIP degradation was found due to the

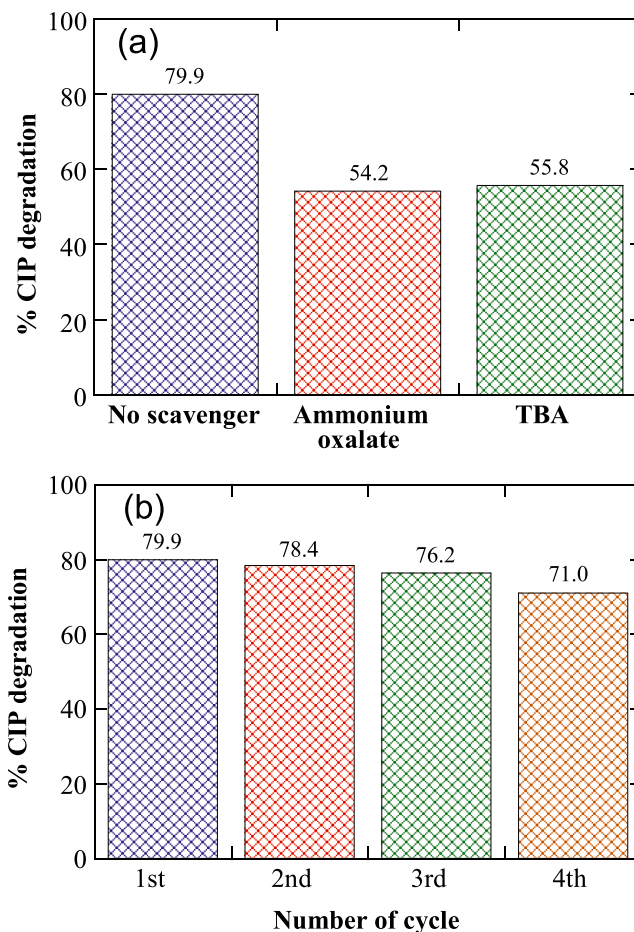


Fig. 5. (a) Effect of 7 mM of ammonium oxalate and 500 mM of *tert*-butanol (TBA) as scavengers over the percentage of CIP degradation after 360 min of electrolysis under the conditions of Fig. 4a, using a 36-W blue LED lamp. (b) Percentage of CIP degradation in four consecutive PEC trials prolonged for 360 min under the conditions of Fig. 4a, using a 36-W blue LED lamp. (For interpretation of the references to color in this figure legend, the reader is referred to the Web version of this article.)

participation of HClO in the oxidative process.

3.5. Reuse of the photoanode material

Reproducible degradation profiles were obtained under either EO or PEC conditions by simply cleaning the final FTO/ZnO/TiO₂/Ag₂Se anode/photoanode surface with Milli-Q water before each new assay, thus ensuring the removal of the adsorbed impurities onto the (photo) active sites. To check the thin film efficiency upon repeated usage, consecutive PEC treatments were carried out with 5.0 mg L^{-1} CIP + 0.070 M NaCl solutions at pH 7.0, 25°C and $E_{\text{an}} = +0.8 \text{ V}$ for 360 min, without cleaning the photoanode. As can be seen in Fig. 5b, CIP degradation decreased by 11% in the fourth trial, i. e., after 1440 min of electrolysis. The EDX and XRD spectra of the photoanode after the prolonged usage were the same as those of the as-synthesized film. This suggests that the loss of performance over time is mainly due to the poisoning of the active centers, probably by the adsorption of the by-products generated, although these compounds can be solubilized when cleaning the electrode surface with pure water.

4. Conclusions

This work demonstrates the feasibility of complete CIP removal, at

concentrations up to 2.5 mg L⁻¹ in 0.07 M NaCl at pH 7.0, employing an FTO/ZnO/TiO₂/Ag₂Se photoanode irradiated with a blue LED lamp and set at $E_{an} = +0.8$ V. This is explained by the reaction between the antibiotic and main oxidants, such as h_{VB}⁺ and [•]OH formed from the photoexcited semiconductor and HClO produced from chloride oxidation. Conversely, the role of physisorbed [•]OH generated by anodic water oxidation is negligible, as can be concluded from the poor degradation under EO conditions. CIP is more rapidly degraded when increasing E_{an} from +0.7 to +1.0 V, as well as when decreasing its initial content from 5.0 to 1.0 mg L⁻¹. However, the antibiotic removal is more efficient at higher concentrations because of the deceleration of the parasitic reactions that waste both [•]OH and HClO. PEC performance is superior when replacing the blue LED light with visible light, owing to the greater photon absorption. The production of h_{VB}⁺ and [•]OH in the PEC process has been confirmed by the inhibitory effect of specific scavengers like ammonium oxalate and TBA, respectively.

CRedit authorship contribution statement

Katherina Changanaqui: Methodology, Investigation, Conceptualization. **Enric Brillas:** Writing – original draft, Validation, Formal analysis. **Pere Lluís Cabot:** Resources, Funding acquisition. **Hugo Alarcón:** Project administration, Funding acquisition. **Ignasi Sirés:** Writing – review & editing.

Declaration of competing interest

The authors declare the following financial interests/personal relationships which may be considered as potential competing interests: Ignasi Sirés reports financial support was provided by State Agency of Research. If there are other authors, they declare that they have no known competing financial interests or personal relationships that could have appeared to influence the work reported in this paper.

The authors declare that they have no known competing financial interests or personal relationships that could have appeared to influence the work reported in this paper.

Data availability

Data will be made available on request.

Acknowledgments

The authors thank financial support from projects PID2019-109291RB-I00 and PID2022-140378OB-I00 (MCIN/AEI/10.13039/501100011033, Spain), co-funded by the EU, as well as from Contract 08–2021 (PROCIENCIA, Peru) for carrying out the research. A special thanks is given to Dr. Maria Fernanda Murrieta, MSc. Pedro Ponce Ortega and MSc. Alejandro Aranda for their support in some preliminary and additional experiments.

References

APWA, 2005. Standard methods for the Examination of water and wastewater, 2005. In: Method Number 4500 – Cl Chlorine (Residual) – G. DPD Colorimetric Method, twenty-first ed. American Public Health Association, Washington D.C, USA. 4-67–4-68.

Botero-Coy, A.M., Martínez-Pachón, D., Boix, C., Rincón, R.J., Castillo, N., Arias-Marín, L.P., Manrique-Losada, L., Torres-Palma, R., Moncayo-Lasso, A., Hernández, F., 2018. An investigation into the occurrence and removal of pharmaceuticals in Colombian wastewater. *Sci. Total Environ.* 642, 842–853. <https://doi.org/10.1016/j.scitotenv.2018.06.088>.

Brillas, E., Garcia-Segura, S., 2023. Recent progress of applied TiO₂ photoelectrocatalysis for the degradation of organic pollutants in wastewaters. *J. Environ. Chem. Eng.* 11, 109635 <https://doi.org/10.1016/j.jece.2023.109635>.

Changanaqui, K., Alarcón, H., Brillas, E., Sirés, I., 2020a. Blue LED light-driven photoelectrocatalytic removal of naproxen from water: kinetics and primary by-products. *J. Electroanal. Chem.* 867, 114192 <https://doi.org/10.1016/j.jelechem.2020.114192>.

Changanaqui, K., Brillas, E., Alarcón, H., Sirés, I., 2020b. ZnO/TiO₂/Ag₂Se nanostructures as photoelectrocatalysts for the degradation of oxytetracycline in water. *Electrochim. Acta* 331, 135194. <https://doi.org/10.1016/j.electacta.2019.135194>.

Chen, R., Xu, D., Guo, G., Tang, Y., 2002. Electrodeposition of silver selenide thin films from aqueous solutions. *J. Mater. Chem.* 12, 1437–1441. <https://doi.org/10.1039/B107177G>.

Cornejo, O.M., Sirés, I., Nava, J.L., 2023. Characterization of a flow-through electrochemical reactor for the degradation of ciprofloxacin by photoelectro-Fenton without external oxygen supply. *Chem. Eng. J.* 455, 140603 <https://doi.org/10.1016/j.cej.2022.140603>.

Divyapriya, G., Srinivasan, R., Mohanalakshmi, J., Nambi, I.M., 2022. Development of a hybrid bifunctional rotating drum electrode system for the enhanced oxidation of ciprofloxacin: an integrated photoelectrocatalysis and photo-electro-Fenton processes. *J. Water Process Eng.* 49, 102967 <https://doi.org/10.1016/j.jwpe.2022.102967>.

dos Santos, A.J., Cabot, P.L., Brillas, E., Sirés, I., 2020. A comprehensive study on the electrochemical advanced oxidation of antihypertensive captopril in different cells and aqueous matrices. *Appl. Catal. B Environ.* 277, 119240 <https://doi.org/10.1016/j.apcatb.2020.119240>.

dos Santos, A.J., Sirés, I., Brillas, E., 2021. Removal of bisphenol A from acidic sulfate medium and urban wastewater using persulfate activated with electrogenerated Fe²⁺. *Chemosphere* 263, 128271. <https://doi.org/10.1016/j.chemosphere.2020.128271>.

Fan, F., Tang, P., Wang, Y., Feng, Y., Chen, A., Luo, R., Li, D., 2015. Facile synthesis and gas sensing properties of tubular hierarchical ZnO self-assembled by porous nanosheets. *Sens. Actuators B Chem.* 215, 231–240. <https://doi.org/10.1016/j.snb.2015.03.048>.

Ge, J.P., Xu, S., Liu, L.P., Li, Y.D., 2006. A positive-microemulsion method for preparing nearly uniform Ag₂Se nanoparticles at low temperature. *Chem. Eur J.* 12 (13), 3672–3677. <https://doi.org/10.1002/chem.200600006>.

Gholami, M., Rasoulzadeh, H., Ahmadi, T., Hosseini, M., 2020. Synthesis, characterization of nickel doped zinc oxide by radio-frequency sputtering and application in photo-electrocatalysis degradation of norfloxacin. *Mater. Lett.* 269, 127647 <https://doi.org/10.1016/j.matlet.2020.127647>.

Govindaraj, R., Santhosh, N., Senthil Pandian, M., Ramasamy, P., 2018. Preparation of titanium dioxide nanorods/nanoparticles via one-step hydrothermal method and their influence as a photoanode material in nanocrystalline dye-sensitized solar cell. *Appl. Surf. Sci.* 449, 166–173. <https://doi.org/10.1016/j.apsusc.2018.01.161>.

Helan, P.P., Mohanraj, K., Sivakumar, G., 2015. Synthesis and characterization of β-Ag₂Se and β-AgCuSe nanoparticles via facile precipitation route. *Trans. Nonferrous Metals Soc. China* 25 (7), 2241–2246. [https://doi.org/10.1016/S1003-6326\(15\)63836-5](https://doi.org/10.1016/S1003-6326(15)63836-5).

Hosseini, M., Esrafil, A., Farzadkia, M., Kermani, M., Gholami, M., 2020. Degradation of ciprofloxacin antibiotic using photo-electrocatalyst process of Ni-doped ZnO deposited by RF sputtering on FTO as an anode electrode from aquatic environments: synthesis, kinetics, and ecotoxicity study. *Microchem. J.* 154, 104663 <https://doi.org/10.1016/j.microc.2020.104663>.

Koiki, B.A., Orimolade, B.O., Zwane, B.N., Nkosi, D., Mabuba, N., Arotiba, O.A., 2020. Cu₂O on anodized TiO₂ nanotube arrays: a heterojunction photoanode for visible light assisted electrochemical degradation of pharmaceuticals in water. *Electrochim. Acta* 340, 135944. <https://doi.org/10.1016/j.electacta.2020.135944>.

Koiki, B.A., Orimolade, B.O., Zwane, B.N., Nkwachukwu, O.V., Muzenda, C., Nkosi, D., Arotiba, O.A., 2021. The application of FTO-Cu₂O/Ag₃PO₄ heterojunction in the photoelectrochemical degradation of emerging pharmaceutical pollutant under visible light irradiation. *Chemosphere* 266, 129231. <https://doi.org/10.1016/j.chemosphere.2020.129231>.

Komtchou, S., Deleghan, N., Dirany, A., Drogui, P., Robert, D., El Khakani, M.A., 2018. Removal of atrazine by photoelectrocatalytic process under sunlight using WN-codoped TiO₂ photoanode. *J. Appl. Electrochem.* 48, 1353–1361. <https://doi.org/10.1007/s10800-018-1253-8>.

Li, W., Liang, R., Hu, A., Huang, Z., Zhou, Y.N., 2014. Generation of oxygen vacancies in visible light activated one-dimensional iodine TiO₂ photocatalysts. *RSC Adv.* 4 (70), 36959–36966. <https://doi.org/10.1039/C4RA04768K>.

Li, Y., Yu, X., Li, R., Zhao, F., Liu, G., Wang, X., 2021. Selective and sensitive visible-light-prompt photoelectrochemical sensor of paracetamol based on Bi₂WO₆ modified with Bi and copper sulfide. *RSC Adv.* 11, 2884. <https://doi.org/10.1039/d0ra08599e>, 2021.

Lin, Y., Li, D., Hu, J., Xiao, G., Wang, J., Li, W., Fu, X., 2012. Highly efficient photocatalytic degradation of organic pollutants by PANI-modified TiO₂ composite. *J. Phys. Chem. C* 116 (9), 5764–5772. <https://doi.org/10.1021/jp211222w>.

Mondal, S.K., Saha, A.K., Sinha, A., 2018. Removal of ciprofloxacin using modified advanced oxidation processes: kinetics, pathways and process optimization. *J. Clean. Prod.* 171, 1203–1214. <https://doi.org/10.1016/j.jclepro.2017.10.091>.

Murrieta, M.F., Brillas, E., Nava, J.L., Sirés, I., 2020. Photo-assisted electrochemical production of HClO and Fe²⁺ as Fenton-like reagents in chloride media for sulfamethoxazole degradation. *Sep. Purif. Technol.* 250, 117236 <https://doi.org/10.1016/j.seppur.2020.117236>.

Nieto-Juárez, J.L., Torres-Palma, R.A., Botero-Coy, A.M., Hernández, F., 2021. Pharmaceuticals and environmental risk assessment in municipal wastewater treatment plants and rivers from Peru. *Environ. Int.* 155, 106674 <https://doi.org/10.1016/j.envint.2021.106674>.

Nkwachukwu, O.V., Muzenda, C., Koiki, B.A., Arotiba, O.A., 2023. Perovskites in photoelectrocatalytic water treatment: bismuth ferrite - graphite nanoparticles composite photoanode for the removal of ciprofloxacin in water. *J. Photochem.*

- Photobiol. Chem. 434, 114275 <https://doi.org/10.1016/j.jphotochem.2022.114275>.
- Orimolade, B.O., Zwane, B.N., Koiki, B.A., Tshwenya, L., Peleyeju, G.M., Mabuba, N., Zhou, M., Arotiba, O.A., 2020. Solar photoelectrocatalytic degradation of ciprofloxacin at a FTO/BiVO₄/MnO₂ anode: kinetics, intermediate products and degradation pathway studies. *J. Environ. Chem. Eng.* 8, 103607 <https://doi.org/10.1016/j.jece.2019.103607>.
- Oriol, R., Sirés, I., Brillas, E., de Andrade, A.R., 2019. A hybrid photoelectrocatalytic/photoelectro-Fenton treatment of Indigo Carmine in acidic aqueous solution using TiO₂ nanotube arrays as photoanode. *J. Electroanal. Chem.* 847, 113088 <https://doi.org/10.1016/j.jelechem.2019.04.048>.
- Palomares-Reyna, D., Carrera-Crespo, J.E., Sosa-Rodríguez, F.S., García-Pérez, U.M., Fuentes-Camargo, I., Lartundo-Rojas, L., Vazquez-Arenas, J., 2022. Photoelectrochemical and ozonation process to degrade ciprofloxacin in synthetic municipal wastewater, using C,N-doped TiO₂ with high visible-light absorption. *J. Environ. Chem. Eng.* 10, 107380 <https://doi.org/10.1016/j.jece.2022.107380>.
- Parsaei-Khomami, A., Mousavi, M., Habibi, M.M., Shirzad, K., Ghasemi, J.B., Wang, L., Yu, J., Yu, H., Li, X., 2022. Highly efficient visible light photoelectrochemical degradation of ciprofloxacin and azo dyes by novel TiO₂/AgBiS₂ photoelectrocatalyst. *Solid State Sci.* 134, 107044 <https://doi.org/10.1016/j.solidstatesciences.2022.107044>.
- Pirhashemi, M., Habibi-Yangjeh, A., Rahim Pouran, S., 2018. Review on the criteria anticipated for the fabrication of highly efficient ZnO-based visible-light-driven photocatalysts. *J. Ind. Eng. Chem.* 62, 1–25. <https://doi.org/10.1016/j.jiec.2018.01.012>.
- Rodríguez, J., Paraguay-Delgado, F., López, A., Alarcón, J., Estrada, W., 2010. Synthesis and characterization of ZnO nanorod films for photocatalytic disinfection of contaminated water. *Thin Solid Films* 519, 729–735. <https://doi.org/10.1016/j.tsf.2010.08.139>.
- Shrinivas, S., Revanasiddappa, M., 2015. Analytical stability indicative method development and validation by high pressure liquid chromatography for assay in ciprofloxacin hydrochloride drug substances. *Am. J. Anal. Chem.* 6, 719–730. <https://doi.org/10.4236/ajac.2015.69069>.
- Someswararao, M.V., Dubey, R.S., Subbarao, P.S.V., 2021. Electrospun composite nanofibers prepared by varying concentrations of TiO₂/ZnO solutions for photocatalytic applications. *J. Photochem. Photobiol., A* 6, 100016. <https://doi.org/10.1016/j.jpap.2021.100016>.
- Wang, J.-T., Cai, Y.-L., Liu, X.-J., Zhang, X.-D., Cai, F.-Y., Cao, H.-L., Zhong, Z., Li, Y.-F., Lü, 2022. Unveiling the visible-light-driven photodegradation pathway and products toxicity of tetracycline in the system of Pt/BiVO₄ nanosheets. *J. Hazard Mater.* 424C, 127596 <https://doi.org/10.1016/j.jhazmat.2021.127596>.
- Wang, T., Xiao, H., Gao, Y., Xu, J., Zhang, Z., Bian, H., Sun, T., 2020. Ag₂O/TiO₂ hollow microsphere heterostructures with exposed high-energy {001} crystal facets and high photocatalytic activities. *J. Mater. Sci. Mater. Electron.* 31, 11496–11507. <https://doi.org/10.1007/s10854-020-03697-w>.
- Zhang, N., Liu, S., Fu, X., Xu, Y.-J., 2011. Synthesis of M@TiO₂ (M = Au, Pd, Pt) core-shell nanocomposites with tunable photoreactivity. *J. Phys. Chem. C* 115 (18), 9136–9145. <https://doi.org/10.1021/jp2009989>.
- Zheng, Z.-H., Zhang, D.-L., Niu, J.-Y., Shi, X.-L., Chen, T.-B., Chen, Y.-F., Li, F., Liang, G.-X., Chen, Y.-X., Fan, P., Chen, Z.-G., 2022. Achieving ultrahigh power factor in n-type Ag₂Se thin films by carrier engineering. *Mater. Today Energy* 24, 100933. <https://doi.org/10.1016/j.mtener.2021.100933>.
- Zhou, Y., Fan, X., Zhang, G., Dong, W., 2019. Fabricating MoS₂ nanoflakes photoanode with unprecedented high photoelectrochemical performance and multi-pollutants degradation test for water treatment. *Chem. Eng. J.* 356, 1003–1013. <https://doi.org/10.1016/j.cej.2018.09.097>.